

CCD star tracker experience -- Key results from Astro J flight

Richard H. Stanton, James W. Alexander and Edwin W. Dennison

Jet Propulsion Laboratory, California Institute of Technology
4800 oak Grove Drive, Pasadena, California 91109

ABSTRACT

Charge-coupled devices (CCDs) have now flown successfully in a number of space scientific and engineering instruments, and have rapidly become the preferred technology for most imaging applications. One of their earliest planned applications in space was in the precision (subarcsecond) star tracker for the Astro series of UV missions. The ASTROS Star "1'racker (AST), designed and build by JPL as a demonstration instrument in the early 80's, and was integrated with the Astro scientific payload in 1985 for a planned March 1986 launch. After a slip of nearly five years, it was finally launched in December 1990, gathering extensive scientific data for over one hundred scientific targets. At least one additional launch is planned, currently scheduled for January 1995.

This paper reviews some of the AS'J' results from the Astro-1 flight. After the five-year stand down, photometric, spectral and geometric calibrations remained virtually unchanged, allowing predictable performance on all targets and successful automatic identification of every star field. Although small changes in the optical point-spread function increased the centroid error, this did not affect operation for Astro, and should be correctable for future instruments. Our data suggest that calibration of centroid error to the 1/100 pixel level is achievable when the point-spread function remains stable. The data are also consistent with the noise-equivalent-angle (NEA) of 1/300 pixels measured in the laboratory for bright stars.

The AST convincingly demonstrated the advantages of using CCDs for star tracking, and in the process helped find many of the scientific targets when the main pointing system developed problems.

1. INTRODUCTION

Developed in part to demonstrate the advantages of CCDs of star-tracking, the AST was finally launched aboard the Astro-1 mission in December 1990. Many of these advantages had already been thoroughly demonstrated on the ground, but a flight was needed to prove that the technology was available for wide application. The performance of the AST on Astro-1 more than justified the early optimism, firmly assuring the dominance of CCDs for space tracking applications in the future.

Originally integrated for the flight that would immediately follow Challenger in early 1986, the Astro-1 ultraviolet astronomy mission was finally launched on STS-35 in December 1990 (Ref. 1). The payload consisted of three large ultraviolet telescopes mounted on the Spacelab Instrument Pointing System (11'S), which provided three-axis control for the acquisition and tracking of scientific targets. Included in the payload was the Image Motion Compensation System (IMCS), designed to accurately compensate the expected line-of-sight disturbances (up to 10-20 arcsecs) caused by crew motion and thruster firing (Ref. 2). Since the IMCS required stellar references accurate to better than one arcsecond, the AST was designed to provide this capability over a field-of-view large enough to provide guide stars for targets anywhere on the celestial sphere.

While the AST performed its IMCS role without difficulty, it ultimately served a role even more vital to the success of Astro-1. By quickly and reliably finding identifiable stars, the AS-J helped overcome a number of significant difficulties experienced by the prime system (Ref. 3). These difficulties included both the inability of the prime trackers (image-dissector based) to find required reference stars, and the failure of onboard Data Display Units (DDU) used by the mission and payload specialists for controlling the instruments. For Astro-1 a backup star identification capability was developed using the AST data that had to be operated from the ground. When the Astro payload is re-flown in January 1995, the capability for automatically identifying acquired stars will be available as a standard operation.

This paper focuses mainly on the in-flight performance of the AST. In particular, the correlation between ground tests performed in 1984, and the flight data taken over six years later indicate that both photometric and geometric calibration can remain stable for years. When added to the other advantages of CCDs (geometric accuracy, ability to measure many images simultaneously, low voltage operation, insensitivity to stray light or magnetic fields, high sensitivity and wide dynamic range, low mass, etc.), there appears little room for image dissectors or photomultipliers in future designs.

2. FLIGHT OVERVIEW

The Astro payload consists of three ultraviolet telescopes, the Hopkins Ultraviolet Telescope (1111'1'), the Ultraviolet Imaging Telescope (UIT) and the Wisconsin Ultraviolet Photo-Polarimeter Experiment (WUPPE), all mounted on the Instrument Pointing System (Figure 1). In addition to the AST, the IMCS consisted of an inertial reference unit, electronics and processor, all of which were integrated and operated by the Marshall Space Flight Center (MSFC).

The mission lasted almost nine days, with 24-hour/day operations conducted in two shifts by two separate crews. Although much of the press coverage was devoted to the problems experienced on the flight, the mission was ultimately declared a complete success, due in significant part to the reliable performance of the AST.

2.1 Planned operation

The acquisition scenario planned to rely on the image dissector trackers provided with the IPS pointing mount to find pre-determined guide stars, and use these as references for repointing to the science target. Once accomplished, this process should place recognizable guide stars within the 1111'1'' or WUPPE field IDs, permitting the Payload Specialist to correctly fine-point the instruments, even if the target itself was not visible. When the target was centered, the IMCS could be activated to stabilize the image, and data collection begun.

Since most targets rose and set in less than one-half of a 90 minute orbit period, it was essential that these steps be completed quickly. Acquiring a target close to the earth's limb paid off in increased observation time..

2.2 Contingency operation

The Mission faced many challenges. The IUS was frequently unable to acquire and track expected guide stars for most targets. This made finding the science target difficult or impossible, particularly given the orbital time constraints. In anticipation of this type of problem, a Contingency Target Acquisition (CTA) process was developed prior to launch. CTA required onboard crew members to identify the stars acquired by the AST using predict field maps and manually repoint based on this identification. After some practice, the crew became adept at performing these operations, and during the first few days the contingency acquisition process looked like it would save a significant fraction of the mission's science return. On Day 4 additional failures threatened even this limited backup capability. One of the two Spacelab Data Display Units (DDU) failed only 9 hours after launch, and the second failed four days into the mission. This meant that not only would all commands have to be loaded from the ground, but also that it was no longer possible for the crew to access the AST star data needed for the CTA process. Fortunately, an additional back-up capability had been developed by one of us (Alexander) that autonomously identified the stars acquired by the AST. During the Astro-1 operations, the ability to automatically calculate the pitch-yaw offsets needed to find the target was added. As soon as AST star data became available to the ground, pointing offsets calculated by this program were relayed by voice to the crew, permitting rapid convergence on the target. Since the AST could acquire stars for all fields, even when pointed a few degrees above the earth's bright limb, this process soon became as fast and reliable as would have been possible had the IPS and DDUs operated nominally.

Despite the significant amount of time lost to these numerous and serious failures, over 200 observations of 135 unique targets were obtained (approximately 68 percent of the maximum expectation). This feat could not have been accomplished without the tireless effort of many individuals onboard and on the ground supporting the flight, and the flawless performance of the AST.

3. TRACKER DESIGN

The AST tracker consists of two major components: the sensor assembly (SA) and electronics assembly (EA). The sensor assembly (Figure 2), included a 250mm focal length f/2.5 lens, a 512x320 RCA CCD, and thermoelectric cooler to stabilized

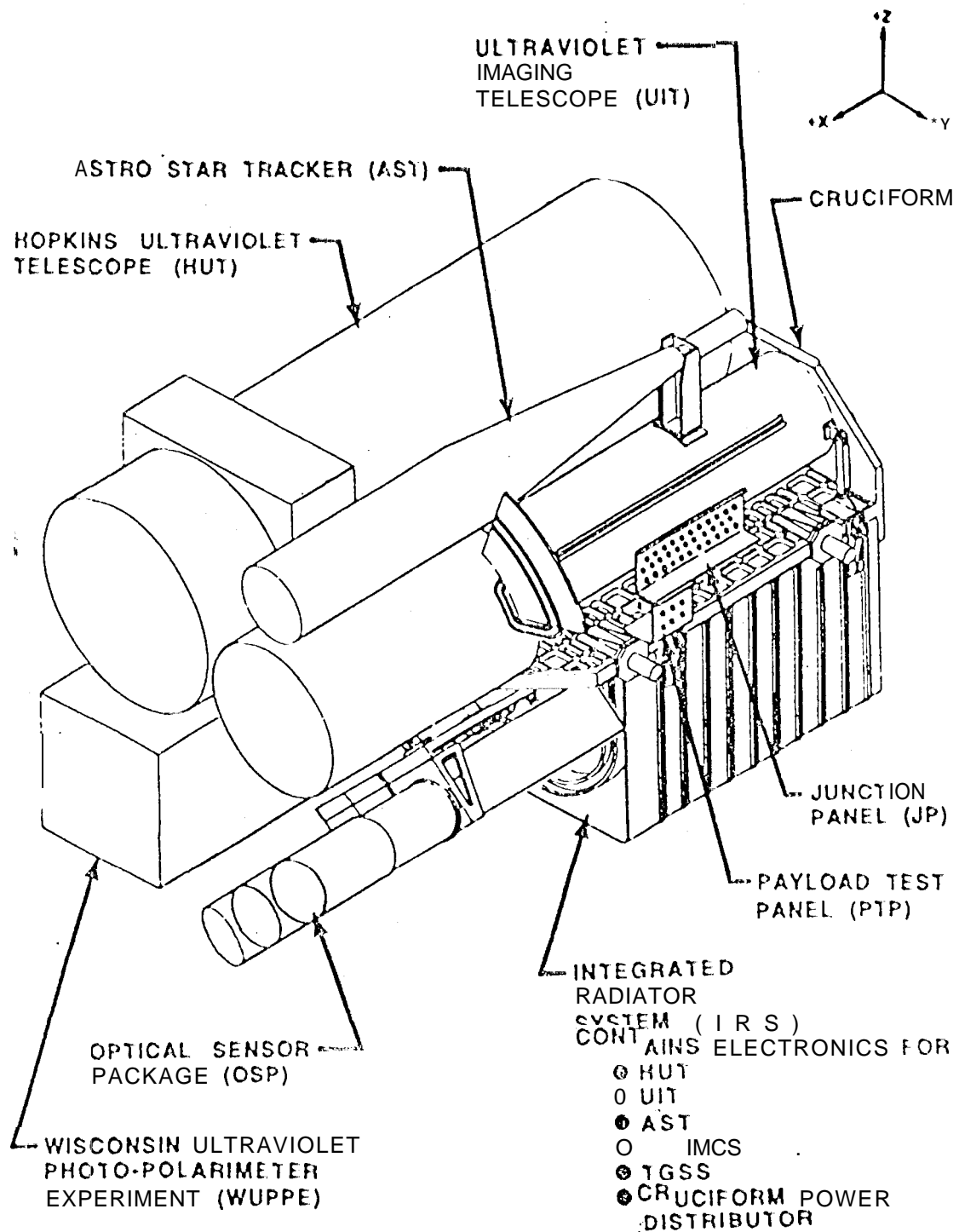
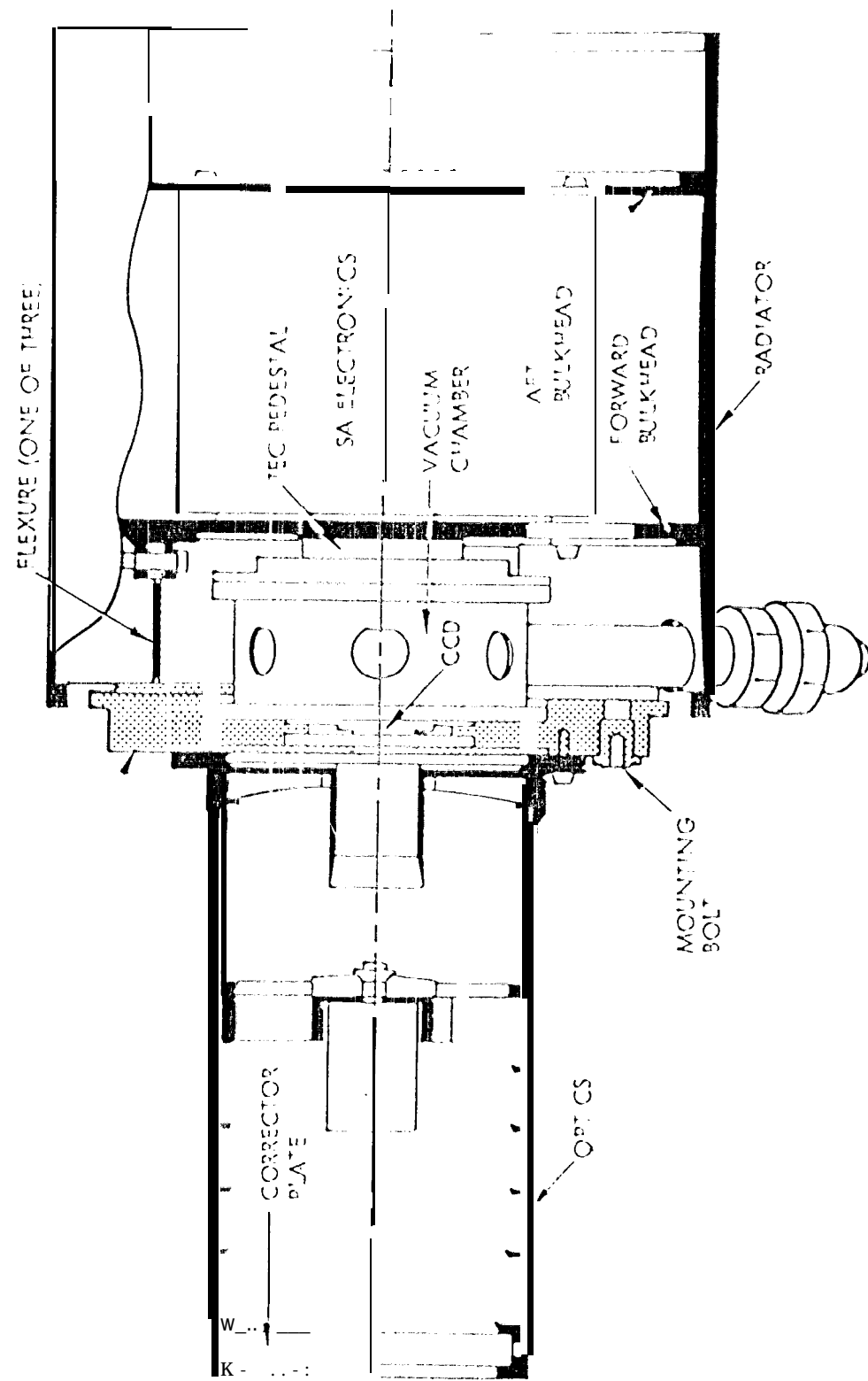


Figure 1

FIGURE 2.0-2. CRUCIFORM/EXPERIMENT ASSEMBLY (SHEET 1 OF 2)

JPL

SENSOR ASSEMBLY



the CCD at approximately -47°C. Either the entire field (2.1x3.5 degrees), or a more limited field (2.1x2.5 degrees), was read during an acquisition sequence, while only selected windows were encoded during tracking. Details of the operating modes, window readout circuitry, and acquisition logic have been described previously (Ref.4-6).

3.1 Requirements and operating modes

In a normal observation sequence, the AST was commanded 10 "operate" after completion of an II'S slew. The tracker initiated the acquisition process evaluating available stars and adjusting the CCD integration time to give best performance for the brightest object in the field. After comparing all candidate stars, up to the three brightest were selected and repeatedly tracked, their brightness and positions sent to the IMCS every second (update rates as high as 8/second could be provided, but were not utilized during the flight). Table 1 provides a summary of the key performance requirements for the AST.

Table 1. AST PERFORMANCE REQUIREMENTS

Probability of Star Acquisition	>97% over entire the celestial sphere
Noise Equivalent Angle	0.3 arcsec 10 (brightest star in FOV)
Small Scale Linearity	0.2. arcsec 10 (motion up 1010 arcsec)
Accuracy Over Full Field	4arcsec 10 (goal 0.8 arcsec)
Update Rate	1 Hz nominal
Star Acquisition Time	<30 sec
Number of Stars Tracked	Up 103
Full Field of View (FOV)	2.2" x 3.5°
Limited Field of View (J,1 'OV)	2.2° x 2.5°
Pixel Size	24.8 x 24.8 arcsec
Output Resolution	18 bits/axis (0.05 arcsec/LSB)
Magnitude Range	-0.8 to +8.2.

3.2 Ground test data

A thorough program of ground testing was implemented since none of the operating algorithms could be changed in flight. Particular attention was paid to the acquisition process to assure that the three brightest stars in the field would be acquired, regardless of whether they were first magnitude or fainter than eighth, or whether as stray light was entering the field, etc. Figures 3 and 4 summarize some of the ground test results (sensitivity versus spectral class and NED versus star brightness) that can be directly related to performance measured during the flight,

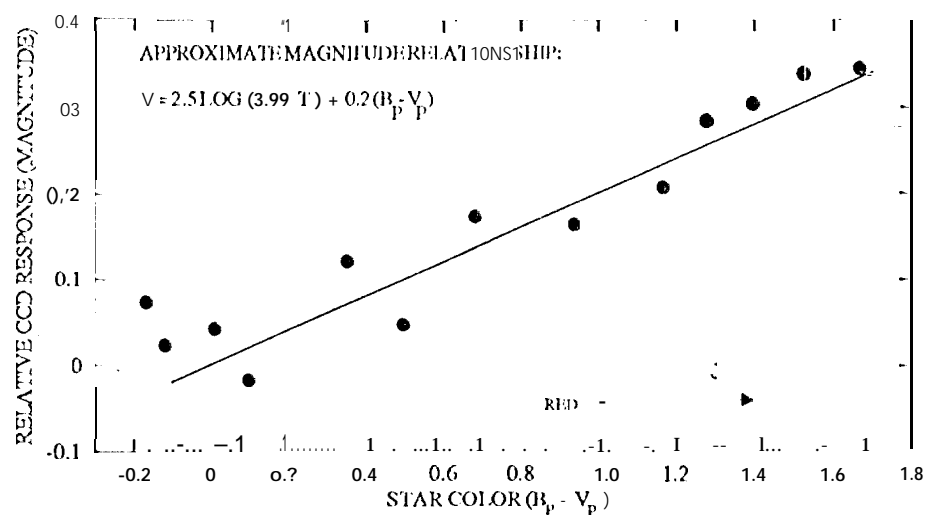
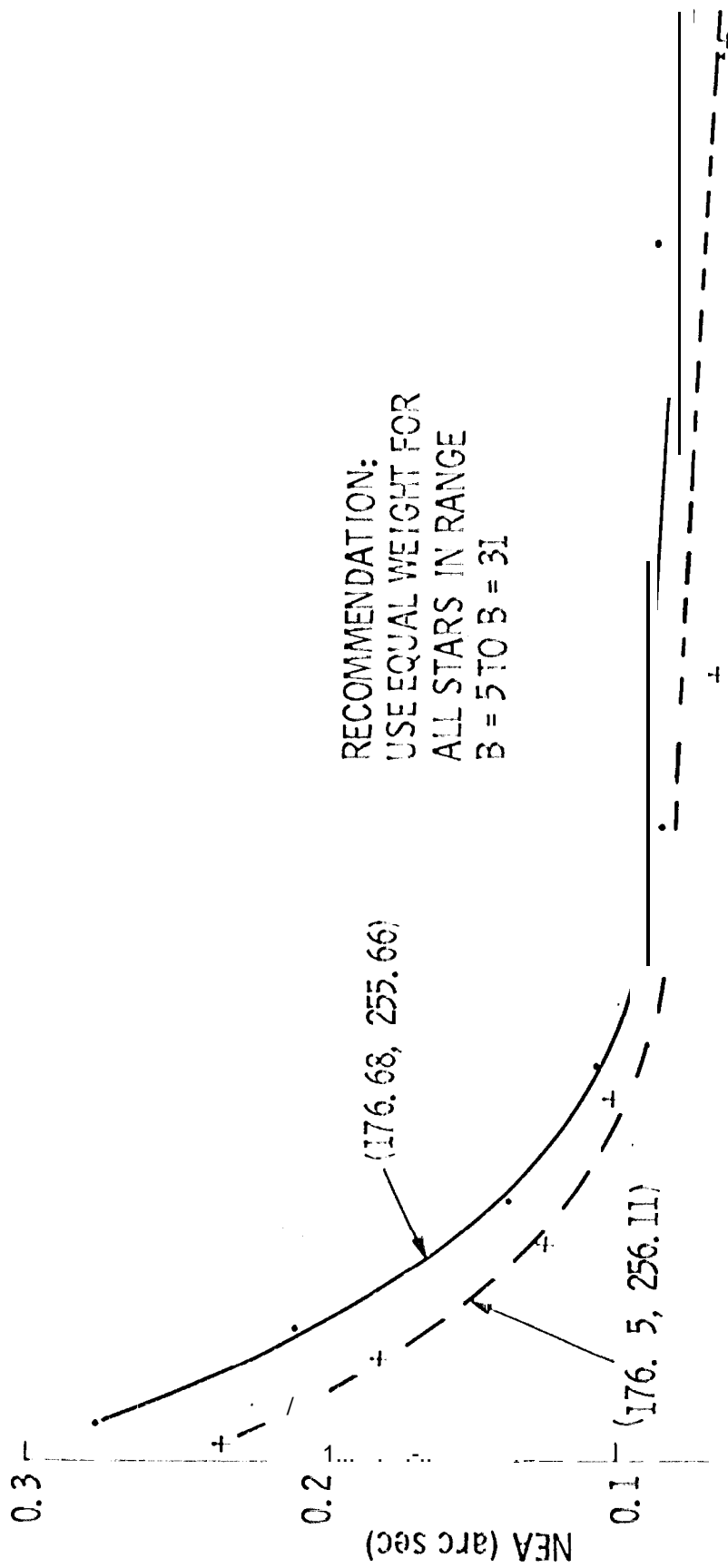


Fig. 3. AST SENSITIVITY VS CLASS (COLOR)

JPL

NEA v S M \leq ASURED BRIGHTNESS



B = BRIGHTNESS NUMBER
OUTPUT BY AST

AST BRIGHTNESS (B)	NEA (arc sec)
4	0.15
5	0.16
6	0.17
7	0.18
8	0.19
9	0.20
10	0.21
15	0.25
20	0.30
25	0.32

4. FLIGHT RESULTS

The on-orbit performance of ASTROSSStar Tracker was essentially flawless, acquiring and tracking stars for every scientific target (with the exception of Jupiter, where only the planet itself was tracked). There were no failed acquisitions over a brightness range greater than 10 stellar magnitudes and as close as 4 degrees from the bright earth limb. Figure 5 shows that targets were acquired over the entire celestial sphere, with the exception of the sun exclusion zone, centered approximately at (55° , -70°).

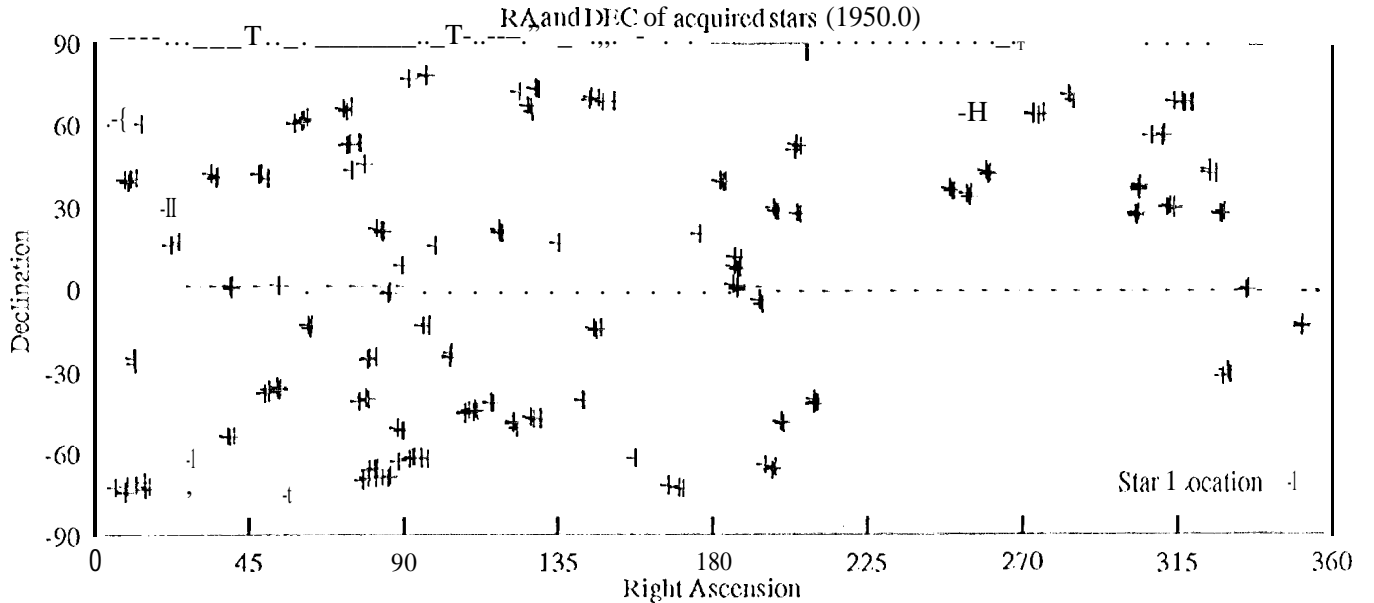


Fig. 5. RA and Dec of stars acquired with the AST during the Astro 1 flight.

4.1 AST-based acquisition

After it was learned that the IUS was not able to reliably acquire many of the desired targets, the acquisition was modified to include the AST in the acquisition loop (in addition to its normal role for the IMCS). A typical observation sequence consisted of the following steps:

- (1) reorienting the shuttle to position the desired target close to the z-axis (normal to the shuttle bay)
- (2) slewing the IPS to the general direction of the science target
- (3) acquiring one to three stars with the AST
- (4) identifying the acquired stars (mostly done automatically on the ground)
- (5) slewing to the desired target based on this identification
- (6) centering the desired target within the science instrument's field
- (7) reacquiring an AST guide star set and beginning the science observation, usually stabilized by the MCS

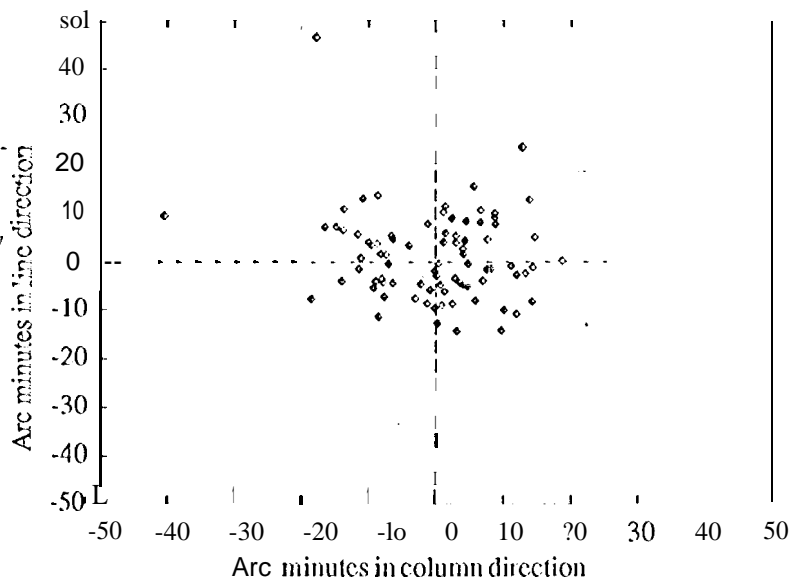


Fig. 6. IPS pointing error at time of As'l' acquisition.

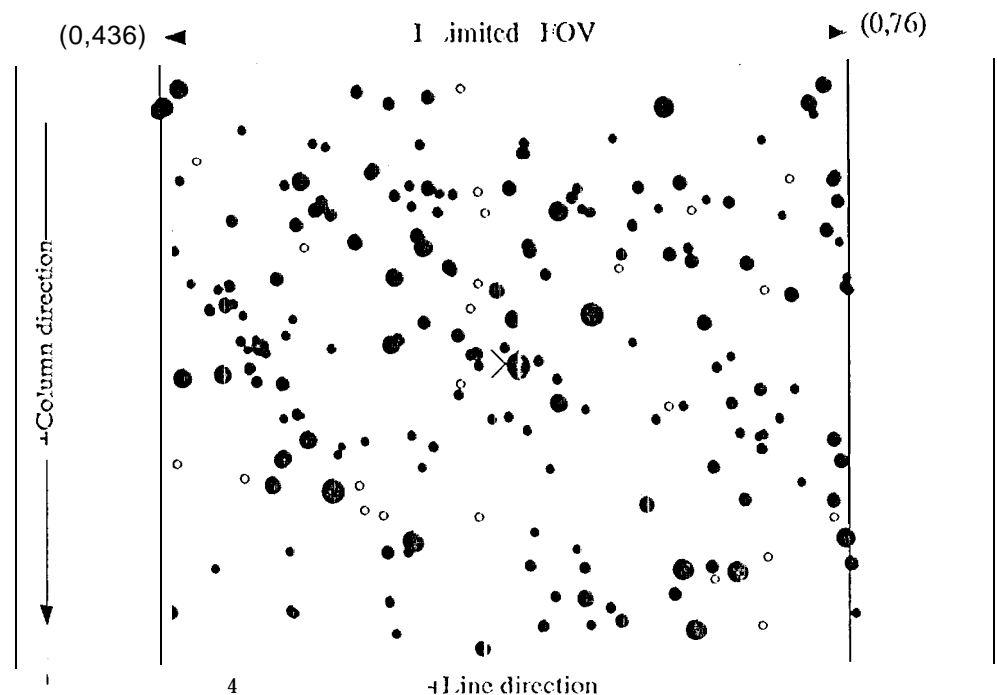


Fig. 7. Locations on the CCD where stars were tracked. The size of the dot is proportional to the magnitude. Magnitude 7.5 and dimmer stars are represented by circles. The full FOV is shown, but stars were only acquired in the limited FOV by command.

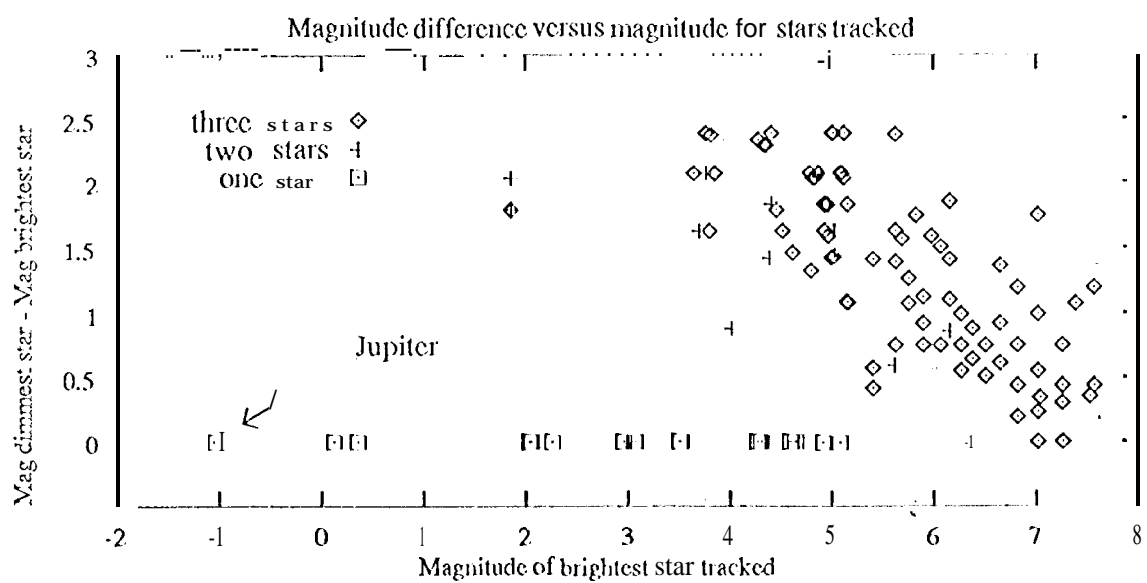


Fig. 8. Range of magnitudes tracked as a function of magnitude.

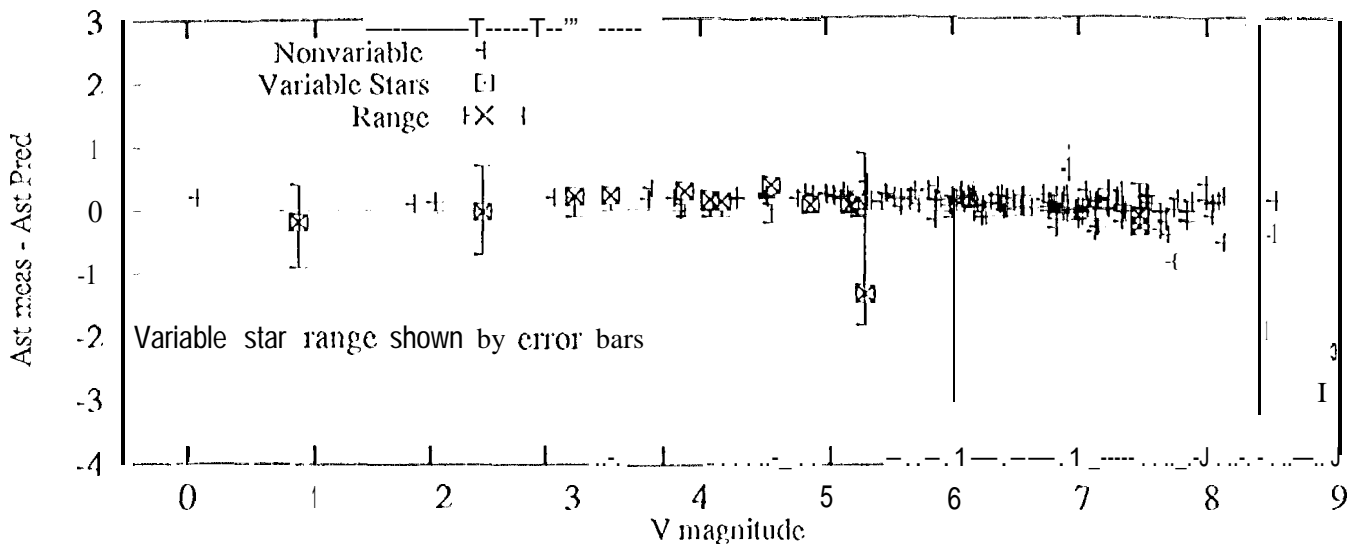


Fig. 9. AST magnitude measurement error shown as a function of visual magnitude

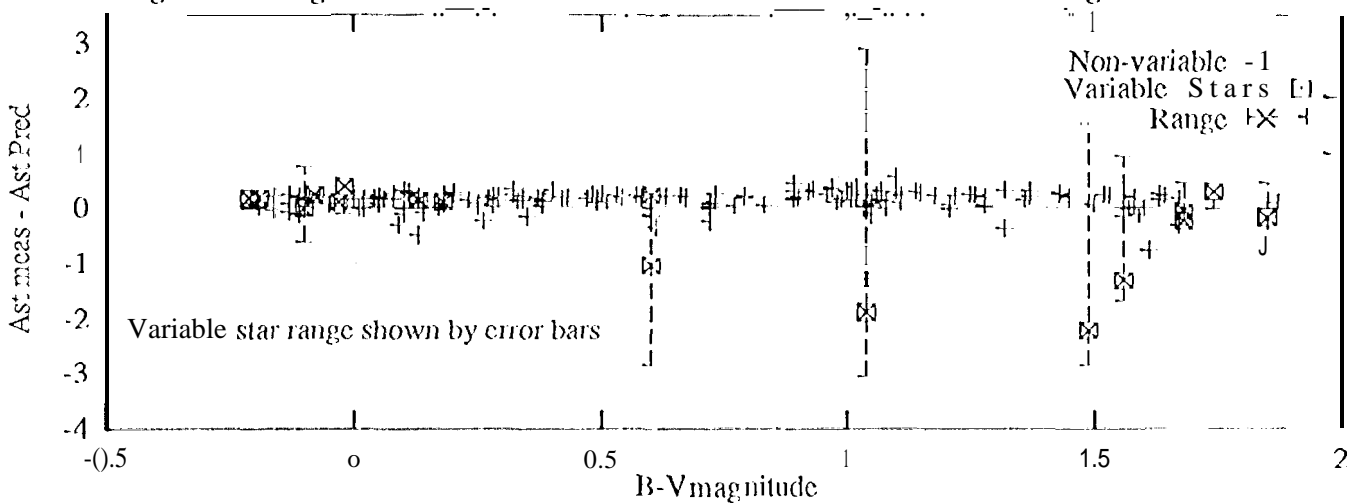


Fig 10. Magnitude measurement ($\text{c}11^{\circ}\text{01}''$) versus star color, expressed by B - V.

Figure 6 shows the initial pointing offset, measured by the AST after the 11'S is pointed generally at the science target (step 2, above). Since the large.st field of view available for acquiring the target in a science instrument was 9×12 arcmin, an initial pointing within 3 arcmin is generally required for reliable identification, unless a large, easily identified target is being sought. As can be seen Figure 6, the initial pointing error was sufficiently large (in some cases almost a degree) that the real-time identification of AS'1'-acquired stars became an essential step in acquiring almost all targets.

4.2 Acquisition statistics

The acquisition of predictable stars by the AST was one of the keys to this entire process. If no stars, or many unexpected stars were acquired, the real-life acquisition of science targets would have been jeopardized. (If an occasional unexpected star, such as a bright variable, was detected it could be easily accounted for and ignored.) The algorithm used for acquisition assumed *no a priori* knowledge of either the brightness of available stars or their distribution across the field. It was required only to find the three brightest stars in the field, regardless of their spatial distribution or brightness, subject only to a limitation that the maximum range in brightness could be no more than 2.5 stellar magnitudes.

Each acquisition consisted of a succession of full-field frames of varying integration time. This allowed the tracker firmware (Reference 6) to (1) rapidly converge on the brightest star, (2) identify the second and third brightest stars (if avail-

able), and (3) evaluate the integration period to give optimum performance for the brightest star. In practice, many of the fields contained no stars brighter than sixth magnitude, so the exposure was limited by the fixed output frame time of one second.

Figure 7 illustrates the location within the field-of-view of all acquired stars during the mission. Although the entire 512x371 pixel field was available (outer rectangle in Figure 7), adequate guide stars could always be found using the inner 37x310 pixels (1 limited FOV) shown as the smaller rectangle, avoiding the considerable image distortion at the field edge. There is no evidence from this Figure of a favored location for acquisition, indicating that the algorithm truly found the "best" guide stars regardless of their location. Similarly, the range of star brightness for all fields where two or three stars were found is consistent with the desired 2.5 magnitude cutoff (Figure 8). Note that if the brightest star is faint (above magnitude 5), the likelihood of having three stars available increases, and the required dynamic range decreases, as expected.

4.3 Magnitude calibration and color correction

Although position, not brightness, was the main discriminator used in identifying star fields, a significant number of fields contained only one star (fainter stars being eliminated by the 2.5 magnitude cutoff). A convincing identification for this case, required a reasonably accurate magnitude calibration. As described in the previous section, calibration as a function of star brightness was performed more than five years prior to launch, based on transfer from direct star measurements made with an engineering model (EM) at the Table Mountain Observatory. CCD quantum efficiency curves showed little variation in the relative spectral response from device to device, so the EM and flight instrument were assumed to be identical in color response.

The engineering model was carefully calibrated using standard photometric techniques to estimate the absorption of the atmosphere as a function of star color (Ref. 7). One result (plotted in Figure 3) was a function to predict the visual magnitude of any star, based on its color ($B_p - V_p$), and brightness as seen by the AST (1' = integration time in msec, B = sensor brightness output calculated by scaling the integrated response of all pixels in the star's image):

$$v = 2.5 \log (3.99 \cdot 1'/11) + 0.2 (B_p - V_p)$$

Figures 9 (Magnitude error vs star brightness) and 10 (Magnitude error vs star color) show the remarkably consistent performance over a wide range of stars. Note that the vertical dashes show the range of variability for known variable stars. Although data scatter increases for fainter stars (due mainly to quantization effects in the linear brightness scale of the AST), star magnitudes can still be easily correlated with corrected catalog values. It can also be seen that the tracker performed linearly over the entire brightness range, with only a small calibration offset (approximately 0.15 magnitude), due mostly to errors transferring calibration from the engineering model to the flight unit. The color response results (Figure 10) validate the

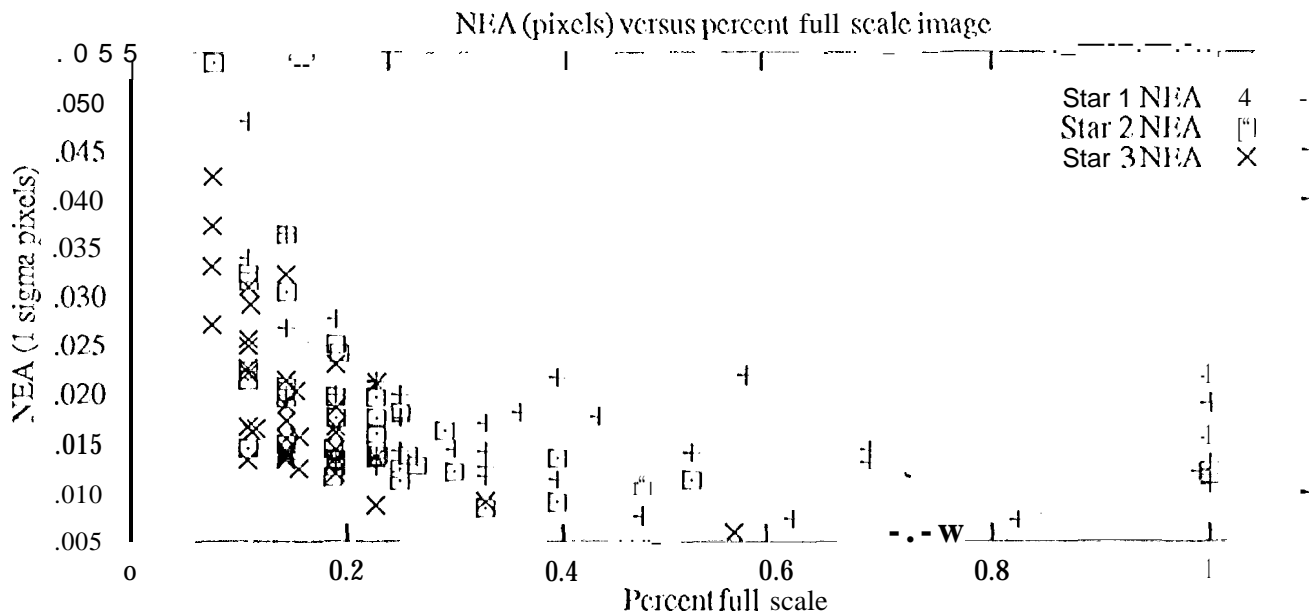


Fig 11. Derived noise equivalent angle based on flight data

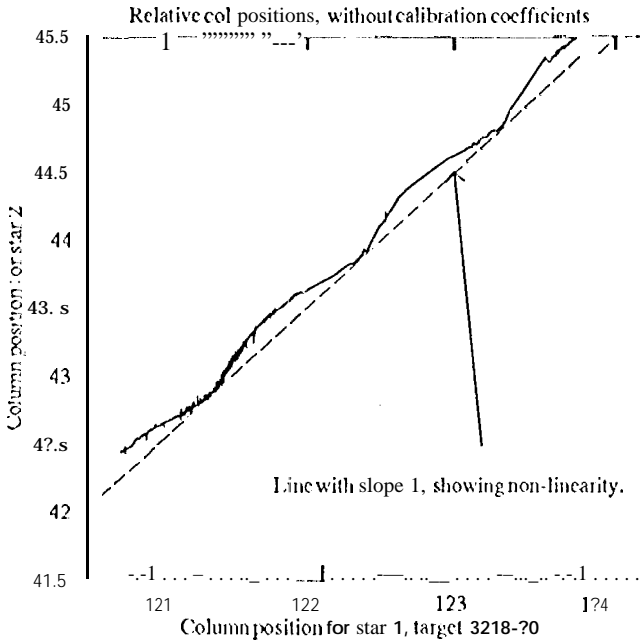


Fig. 12 Uncorrected centroid

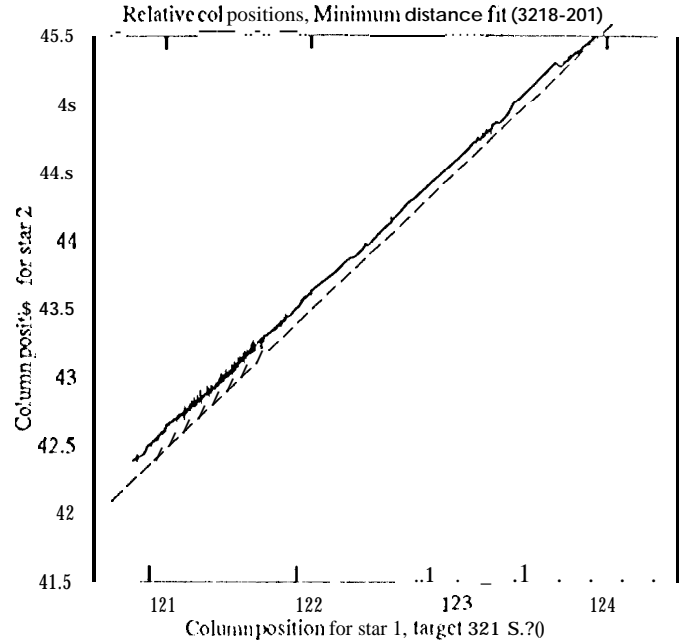


Fig. 13 Centroid after post-flight correction

assumption that there was little difference between the CCDs used, suggesting that a single calibration might well suffice for an entire production run of trackers.

4.4 Noise equivalent angle

Extracting tracker performance in the presence of significant line-of-sight motion experienced during the flight (often 5-10 arcsec in amplitude) required the comparison of simultaneous data from two or three stars (Ref. 8). For stationary, bright star images in the laboratory, a noise-equivalent angle of roughly .003 pixel (.07 arcsec) was consistently measured. Figure 11 shows that significantly higher NEA was measured during the flight, although it was well below 0.5 arcsecs for even faint stars. The fact that Star 3 (faintest in the field) generally exhibited the lowest NEA suggests residual contributions from line-of-sight motion are still present in these data.

4.5 Measurement accuracy

In order to study tracker accuracy over small (<100 arcsec) image displacements, boresight motion during the observation, as well as tracking two or more stars, were required. One such case, the observation of Comet Levy, was studied in detail. When the observation began, three stars were acquired, located approximately at the following (line, column) coordinates: (120,185), (160,35) and (405,40). As the comet moved, each star tracked across roughly three CCD columns and lines, giving excellent data on small scale errors in the centroid calculation. As in the NEA case, the large, common motion of the boresight had to be eliminated before the centroid errors became apparent.

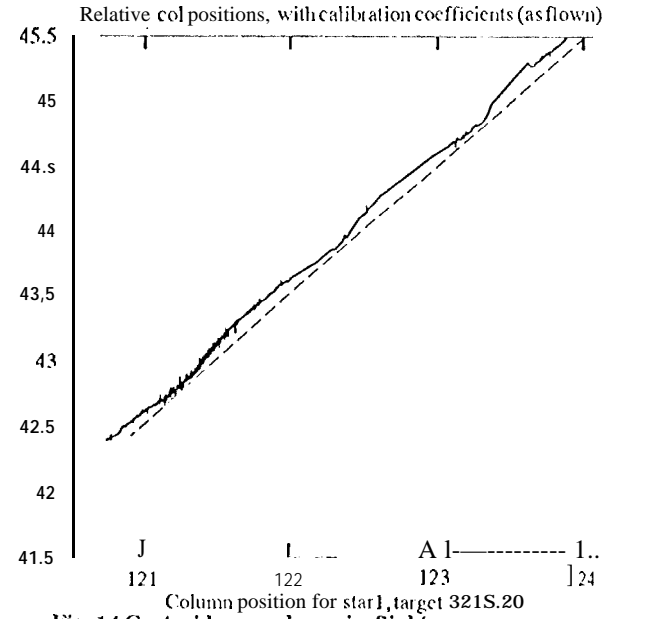


Fig. 14 Centroid error shown in-flight

Figures 12, 13 and 14 display the result. Without any linearization of the centroid algorithm, a peak-to-peak error of roughly 1/10 pixel is observed in the worst case (stars near the field edge, errors for both stars adding in phase.). With appropriate selection of calibration coefficients these errors can be reduced by an order-of magnitude (Figure 13). Since the stability

of this calibration depends critically on the stability of the star image point-spread function, we experienced considerable centroid error with the coefficients actually flown (Figure 14). It should be possible to achieve performance commensurate with that shown in Figure 14 with extensive ground calibration and very stable optics, or perhaps using in-flight calibrations at several points across the field.

5. CONCLUSIONS

The Astro-1 flight provided a wealth of data corroborating the many significant advantages predicted for CCD-based star tracking. The photometric, geometric and spectral performance remained essentially unchanged over the five year launch delay that was experienced. The best guide stars were automatically found for all 135 science targets, implying that failed star acquisitions need be no longer a concern to mission planners. With the combination of high accuracy, both geometric and photometric, and virtually certain acquisition of identifiable stars, the AST has helped usher in a new era in star tracking.

6. ACKNOWLEDGEMENTS

The authors are grateful to the entire AST development team at JPL, for the many long hours and dedicated effort required for achieving this success. We also thank the Astro-1 team at the George C. Marshall Space Flight Center for their close support and cooperation through the development, stand-down, and flight stages of the project.

The research described in this paper was carried out by the Jet Propulsion Laboratory, California Institute of Technology, under a contract with the National Aeronautics and Space Administration.

7. REFERENCES

1. A. F. Davidsen, "Far-Ultraviolet Astronomy on the Astro-1 Space Shuttle Mission", *Science*, Vol. 259, pp 327-334, 15 January 1993.
2. J. J. Deily and F. H. Bauer, "Flight Performance of a Shuttle-based Image Motion Compensation System for the Ultraviolet Imaging Telescope", *AIAA Guidance and Control Conference*, August, 1992.
3. "Astro-1 Mission Flight Evaluation Report", George C. Marshall Space Flight Center, Huntsville, Alabama, February 28, 1991.
4. R. H. Stanton et. al., "ASTROS: A Sub-arcsec CCD Star Tracker", *SPIE/Vol. 501 State of the Art Imaging arrays and Their Applications* (1984).
5. R. H. Stanton et. al., "Optical Tracking using Charge-Coupled Devices", *Optical Engineering*, Vol. 26, No. 9, p.930-938, Sept. 1987.
6. E. Shalom et al, "Acquisition and Track Algorithms for the ASTROS Star Tracker", *Annual Rocky Mountain Guidance and Control Conference*, Paper A AS 85-050,
7. Keystone, Colorado, Feb. 1986.
W. B. Harris, "Photoelectric Photometry: An Approach to Data Reduction", *Pub. of the Astronomical Society of the Pacific*, p. 507-517, August 1981.
8. J. W. Alexander, "ASTROS Star Tracker Performance Evaluation Report for the Astro-1 Mission", JPL D-8129, June 1992.